

From Experiments to Expertise: Scientific Knowledge Consolidation for AI-Driven Computational Research

Haonan Huang^{1,*}

¹Department of Physics, Princeton University, Princeton, NJ, USA

*Correspondence: hnhuang@princeton.edu

Abstract

While large language models have transformed AI agents into proficient executors of computational materials science, performing a hundred simulations does not make a researcher. What distinguishes research from routine execution is the progressive accumulation of knowledge — learning which approaches fail, recognizing patterns across systems, and applying understanding to new problems. However, the prevailing paradigm in AI-driven computational science treats each execution in isolation, largely discarding hard-won insights between runs. Here we present QMatSuite, an open-source platform closing this gap. Agents record findings with full provenance, retrieve knowledge before new calculations, and in dedicated reflection sessions correct erroneous findings and synthesize observations into cross-compound patterns. In benchmarks on a six-step quantum-mechanical simulation workflow, accumulated knowledge reduces reasoning overhead by 67% and improves accuracy from 47% to 3% deviation from literature — and when transferred to an unfamiliar material, achieves 1% deviation with zero pipeline failures.

Introduction

AI agents can now autonomously plan, execute, and interpret computational materials science simulations, in many cases matching the proficiency of trained researchers on simulation tasks of various complexity [1–12]. The execution problem — can AI run quantum material simulations correctly? — is largely solved.

But execution is not research. A researcher who performs a hundred calculations over six months does not simply accumulate a hundred results. They internalize technical nuances, distinguish physical reality from artifacts, and distill cumulative observations into general principles. This progressive transformation of experience into expertise is what current AI systems lack. Existing agents start each session without access to findings from previous sessions: cross-session knowledge is either architecturally absent, limited to session-scoped scratchpads that reset between runs, or consists of static rules curated by human experts [4, 9, 10]. RAG from calculation logs provides a partial remedy but lacks mechanisms for quality validation, knowledge abstraction, and traceable provenance [13]. Recent surveys have identified experiential accumulation and consolidation as a critical frontier for AI agents broadly [14], but in computational science the gap remains entirely open.

This gap will not close by building smarter models. The issue is structural: an agent session lasts minutes to hours, a research program unfolds over months to years. Bridging this requires infrastructure — a platform where findings from one session are available to the next, where those findings can be reviewed and corrected, and where accumulated observations can be synthesized into higher-order understanding.

Here we present QMatSuite, an open-source computational materials science platform built to provide this infrastructure. We validate it across 135 autonomous solid-state calculations spanning six material categories and 98 molecular geometry optimizations — using two different AI models and three simulation engines — and through a controlled learning-curve experiment on a complex six-step anomalous Hall conductivity workflow where accumulated knowledge transforms both the efficiency and the character of the agent’s work, transferring successfully to an unfamiliar material. We demonstrate that knowledge consolidation requires dedicated reflection sessions separate from task execution — paralleling the cognitive rhythm of human research. The platform supports 15 simulation engines and connects to any AI model via the Model Context Protocol [15], decoupling accumulated scientific knowledge from both the computational engine that produced it and the AI model that will use it.

Results

Platform design and scale validation

QMatSuite is built on three core pillars. First, it abstracts simulation complexity through engine-agnostic structured tools (`set_parameters`, `run_calculation`, `get_results_summary`), translating high-level agent calls into engine-specific inputs for 15 simulation codes (Extended Data Table 1). Both AI agents (via MCP) and human researchers (via a desktop GUI) access the same core through unified public API (Fig. 1a).

Second, the platform ensures reproducible research through a conventional file system for storage, while end-to-end provenance tracks the entire history from raw inputs to final insights. This creates an auditable chain from raw data to derived insight, in the spirit of reproducible workflow infrastructures [16–18].

Third — and central to this work — the platform provides a persistent scientific memory system. Knowledge entries are organized in a graded hierarchy: *findings* record observations from individual calculations (“PBE overestimates the GaAs lattice constant by 1.6%”), *patterns* synthesize regularities across multiple findings (“PBE overestimation scales with atomic mass across III-V compounds”), and *principles* encode general rules. The knowledge base comprises three distinct libraries: curated best practices (read-only), agent-generated insights that accumulate across sessions (read-write), and community knowledge packs that research groups can publish and share. We will focus on the agent-generated knowledge pipeline in this paper.

Because calculation execution naturally consumes the agent’s full attention, the platform does not rely on the agent spontaneously pausing to manage knowledge. Instead, it embeds reminders at natural workflow junctures: tool preambles prompt the agent to search prior knowledge before configuring a new calculation; post-execution return messages prompt it to record error-recovery findings; and results summaries prompt it to log numerical outcomes. These lightweight nudges — delivered through the standard MCP tool interface automatically — make knowledge bookkeeping a natural byproduct of the calculation workflow rather than a separate task (Supplementary Note 1). The efficiency of such nudging mechanism is tested directly in the experiments below.

All experiments in this work are driven by short natural-language prompts specifying only scientific intent (reproduced verbatim in each figure banner). Agents receive no guidance on computational parameters, software syntax, or workflow structure, demonstrating the robustness and universality of the system design (Supplementary Note 1).

Scale validation. To validate the platform at scale, we deployed an autonomous agent (Claude Sonnet 4.6) via the QMatSuite’s MCP interface to drive structural relaxations and band structure

calculations in Quantum ESPRESSO (QE) [19, 20]. Testing across 135 diverse materials spanning six categories (elemental metals and semiconductors, binary semiconductors, simple oxides, halides, layered transition metal compounds, and topological insulators) (Fig. 1b,c) yielded an 85.2% autonomous completion rate (115 materials). Success rates scaled with structural complexity, from 100% in simple metals to 62–65% in topological insulators and layered transition metal compounds. Notably, the 20 incomplete cases resulted exclusively from timeouts rather than crashes or erroneous outputs.

Lattice constants for 114 materials agree with experiment at 1.02% mean absolute error (MAE), consistent with established PBE benchmarks [21]. Band gaps for 68 non-metallic compounds show 1.76 eV MAE, dominated by the expected PBE underestimation. All 42 metals were correctly identified; five strongly correlated insulators (α -Sn, CdO, VO₂, LaMnO₃, CoO) were predicted metallic — known semilocal-DFT failures, not agent errors [22, 23]. The agent recorded a median of 3 insights per material, searching prior knowledge 4.2 times and recording 3.2 times on average — confirming that the platform’s nudge-based knowledge bookkeeping integrates naturally into the calculation workflow without explicit user instructions.

Cross-engine and agent validation. To verify engine and model agnosticism, we deployed GPT 5.4 (OpenAI) with ORCA 6.1.1 [24] for 98 molecular geometry optimizations (Extended Data Fig. 2), among which 91 molecules completed successfully. Bond lengths for the reference-backed raw-ORCA-converged subset agree with spectroscopic references at MAE = 0.0069 Å (0.52%), and bond angles at MAE = 0.51°, consistent with established hybrid-DFT geometry benchmarks [25, 26]. The seven final failures comprise two agent-declared failures despite converged raw outputs, three missing or non-terminated last-output cases, and two explicit last-attempt error terminations.

Knowledge transforms a complex workflow

The learning curve

The 135-material validation demonstrates competence on routine computational tasks. The more demanding test is whether accumulated knowledge helps when task complexity exceeds what pre-training alone can handle — when parameters must be coordinated across multiple codes, failure modes are undocumented, and physical judgment is required at multiple steps. We chose the anomalous Hall conductivity (AHC) of bcc iron as the testbed: a quantum-mechanical transport property [27] whose computation requires a six-step pipeline coupling two simulation codes (QE and Wannier90 [28]), with a large parameter space where many settings require non-trivial physical reasoning. Even experienced practitioners require significant trial and error; the literature value is approximately -751 S/cm [29].

We ran the identical task three times in sequence (Fig. 2), each as a fresh session with a fresh project directory and the same model (Claude Opus 4.6). The sole variable carried between runs was the knowledge database: the baseline started empty, the second run inherited 6 insights from the first, and the third inherited 9.

Every metric improves monotonically (Fig. 2a). API reasoning time — which isolates cognitive effort from simulation compute — dropped from 42.8 to 16.1 minutes (62% reduction), total tool calls from 251 to 143, and pipeline execution attempts from 23 to 10. AHC accuracy improved from -1100 S/cm (46.5% error) to -846.2 S/cm (12.7%) to -771.5 S/cm (2.7%).

The dominant time saving traces to a single insight. In the baseline, the agent spent around 3 hours and 14 pipeline attempts diagnosing why the computed AHC was zero — ultimately discovering that QE’s non-self-consistent (NSCF) step requires explicit non-zero `starting_magnetization`;

otherwise, it silently defaults to a non-magnetic state, producing zero Berry curvature and zero AHC. This behavior — physically counterintuitive because NSCF reuses converged charge densities — is neither clearly documented in standard manuals nor represented in training data. The finding was recorded as insight #2. In both subsequent runs, the agent retrieved this insight before its first calculation and applied the fix proactively, entirely eliminating the debugging episode (Fig. 2b).

Three observations establish the knowledge database, rather than pre-training knowledge, as the causal variable (Extended Data Table 3). First, the identical model without the database required 14 attempts and 3.5 hours to discover the spin initialization requirement. Second, the third run failed to retrieve an available insight and consequently re-encountered the corresponding error — demonstrating that retrieval, not latent model knowledge, mediates transfer. Third, the monotonic improvement across three runs with identical model weights but increasing database content is consistent only with the database as the independent variable.

Cognitive liberation

Total wall time does not monotonically decrease — and this tells the most interesting story. The baseline agent finished at 6.2 hours, most of it consumed by infrastructure debugging; it never had the opportunity to question whether its result was converged. The second run completed in under two hours but also did not attempt convergence optimization. The third run reached its first valid result (-921 S/cm, 23% error) in 58 minutes — then voluntarily spent an additional 19 hours on a systematic seven-iteration convergence study, varying disentanglement parameters and comparing uniform versus adaptive mesh refinement strategies. It discovered that adaptive refinement outperforms brute-force mesh densification at one-seventh the computational cost — a genuine methodology insight that no previous run had the cognitive bandwidth to pursue.

The three runs thus exhibit a qualitative behavioral progression (Fig. 2c and Extended Data Fig. 1): from debugger (the baseline, spending 70% of tool calls on infrastructure), through solver (the second run, resolving known and novel errors to reach a valid result), to optimizer (the third run, freed from debugging to pursue systematic physical exploration). The accuracy improvement from 47% to 3% is a consequence of this liberation, not of the knowledge system directly optimizing parameters.

Knowledge quality and self-correction

Across three runs, the agent accumulated 15 insights (Extended Data Table 2): 9 error-recovery findings (60%), 3 result recordings (20%), and 3 methodology insights (20%) — the last category appearing only in the third run, reflecting the behavioral shift toward physics exploration. Of the 15, 13 are fully correct, one is partially correct, and one contains correct data but an incorrect conclusion. This last case involves Wannier90’s disentanglement parameter `dis_froz_max`, which sets the upper energy boundary of the “frozen window” — the range within which Bloch states are included exactly in the Wannier representation [30]. For transport properties that depend on states near the Fermi level, this window should extend well above the Fermi energy to ensure accuracy of relevant bands. The agent’s third run found that setting `dis_froz_max` to 17 eV (slightly below the Fermi energy of ~ 17.5 eV) gave the best AHC value and recommended keeping it low — prioritizing an accidental fit to literature over rigorous convergence validation (Fig. 3a).

In a dedicated review session, the same model operating in reflection mode identified this error (Fig. 3a). Applying convergence analysis to the agent’s own parameter sweep data, it recognized that the recommended value was an unconverged outlier while higher values produced stable results. It further verified this against official tutorial input files retrieved from raw source repositories,

which directly contradicted the calculation agent’s recommendation. The insight was deprecated and replaced with a corrected version citing both the convergence data and the tutorial evidence. This self-correction required structured general guidance, but the agents find answers themselves (Supplementary Note 3).

Cross-material transfer

To test whether knowledge generalizes beyond the material that produced it, we applied the reviewed iron knowledge database (21 insights) to a nickel AHC calculation — a system with no prior entries in the database. The prompt was identical except for the element name (Fig. 3b,c).

The agent completed the Ni AHC in 66 tool calls with only 3 pipeline executions — all successful — achieving $|\sigma_z| = 2079$ S/cm (within 1.0% deviation from the literature value of ~ 2073 S/cm [31]). API reasoning time was 14.1 minutes. The agent proactively applied correct pseudopotentials, spin settings, and convergence strategies from iron knowledge.

A controlled three-way Ni comparison shed light on the effect of knowledge quality (Fig. 3b,c). The naive baseline agent (0 insights) required 14 pipeline executions — 7 failures — and 272 tool calls to reach $\sim 5\%$ error. The agent with 15 unreviewed Fe insights reduced this to 9 executions but inherited an incorrect parameter recommendation, costing three additional iterations, but the agent can still recover from such knowledge poisoning. The reviewed 21-insight agent completed the task in 3 executions with zero failures.

The most revealing finding concerns what did *not* transfer. Without prior nickel calculation record, the 21-insight agent could not engage in recipe replication — the behavior observed in all six same-material iron sessions (Supplementary Note 3), where a key parameter was copied verbatim from the highest-performing prior result despite being flagged as incorrect. For nickel, it instead reasoned from general principles, arriving at a physically correct parameter choice. Strikingly, the same agent achieved better accuracy on an unfamiliar material (1.0%) than on the familiar one (16–23% in same-material reruns). While the Ni result may partly reflect favorable error cancellation in the absence of a systematic convergence study, the contrast suggests that recipe availability can actively hinder principle-based reasoning.

Knowledge consolidates into understanding

From findings to patterns

The AHC experiments demonstrate that accumulated findings improve efficiency and accuracy on a single complex workflow. A natural next question is whether agents can move beyond individual findings to synthesize higher-order understanding — recognizing regularities that span multiple calculations and materials. To test this, we ran a chain of 24 calculation sessions across 19 zinc-blende semiconductors, during which the agent accumulated 25 individual findings — each a structured record of one calculation’s outcome (e.g., “PBE overestimates the GaAs lattice constant by 1.6%”). No higher-order synthesis occurred during any task-execution session: across 398 execution sessions, 84.9% received the platform’s recording nudges, yet 95.3% of all knowledge recordings occurred in end-of-session batches and zero pattern-grade entries — cross-compound generalizations that synthesize multiple findings — were produced (Fig. 4b,c). Trace analysis reveals that agents informally recognized cross-compound trends during execution, yet never deposited these as higher-grade knowledge entries, because attention was fully consumed by the current calculation.

A dedicated reflection session with a 12-word prompt (“Review accumulated findings and summarize any patterns you see across compounds”) produced three quantitative patterns from 25 individual

findings in under three minutes (Fig. 4a). Pattern 1 identified that PBE lattice constant overestimation scales systematically with atomic mass across all three compound families (Group IV, III-V, II-VI), with quantitative error ranges tabulated per family — a synthesis spanning 19 compounds that no single session could have produced. Pattern 2 distinguished quantitative band gap underestimation from qualitative topological failures in near-zero-gap systems. Pattern 3 established that variable-cell relaxation with semicore pseudopotentials requires kinetic energy cutoffs above 80 Ry, supported by 13 successful calculations with Pulay stress identified as the causal mechanism [32]. Each pattern references its supporting findings by unique identifier, maintaining full provenance to source calculations. These are not trivial restatements — they contain structured quantitative data, causal reasoning, and explicit scope boundaries.

An independent session using a less capable model (Claude Sonnet 4.6 instead of Opus 4.6) produced three patterns with identical themes from the same 25 findings, confirming that pattern structure is latent in the data rather than an artifact of a specific model.

This parallels a well-established observation in human cognition: synthesis does not occur during task execution but requires dedicated reflective activity [33, 34]. Independently, recent work on experiential reinforcement learning has identified an analogous reflection-consolidation loop as necessary for durable improvement in AI agents [35]. Our findings provide empirical evidence for this principle in a scientific computing context.

From understanding to new inquiry

As a proof of principle, we prompted the agent to test one of its patterns. It selected InP, predicted a PBE band gap of ~ 0.7 eV by interpolating Pattern 2’s underestimation trend, and computed 0.696 eV — confirming the prediction. While this amounts to interpolation along a monotonic curve, it demonstrates that the full knowledge cycle — from observation through consolidation to hypothesis-driven inquiry — can close autonomously. Whether agents can design more physically creative experiments from richer knowledge bases remains an intriguing open question for future work.

Discussion

The experiments presented here demonstrate that persistent scientific memory transforms AI agent behavior beyond simple acceleration. The learning curve shows the most visible effect — a 67% reduction in reasoning overhead from baseline to cross-material transfer — but the deeper transformation is qualitative. The runs exhibit a behavioral progression from debugger to solver to optimizer to transferable expert: the baseline agent spent its entire session on infrastructure; the knowledge-equipped agent on an unfamiliar material completed the task with zero pipeline failures.

Agent-generated knowledge is predominantly correct, demonstrating that the recording system produces reliable scientific documentation. Like any research output, it occasionally captures incorrect conclusions: the `dis_froz_max` recommendation was based on correct numerical data but drew the wrong inference from under-converged calculations. Critically, unreviewed incorrect knowledge has measurable cost: the 15-insight Ni agent required 3 extra iterations to override inherited bad advice, while the reviewed 21-insight agent encountered zero failures. This establishes knowledge review not as an academic exercise but as a practical necessity that measurably reduces wasted computation.

The knowledge system directly addresses the RAG limitations [13, 36, 37] identified in the Introduction, with our experiments providing direct evidence for each. Regarding correctness, unreviewed knowledge containing flawed recommendations results in performance penalty; the reviewed database

eliminated this cost entirely. For compression, 25 individual findings were consolidated into 3 patterns in under three minutes; such abstraction renders retrieval and community sharing trivial due to the reduced data footprint. Finally, concerning provenance, when the review session deprecated the `dis_froz_max` recommendation, the system preserved the complete lineage from the erroneous conclusion back to the source data, ensuring the correction remained fully auditable and verifiable.

Agents exhibit distinct cognitive modes that have direct implications for system design. In execution mode, agents are goal-directed and resistant to mid-task reflection — only 4.0% of sessions show any mid-session knowledge recording despite 84.9% receiving explicit nudges, and zero pattern-grade entries were produced across 398 sessions. In reflection mode, the same model performs convergence analysis, tutorial verification, and self-correction [38, 39]. Effective AI research programs should alternate between execution and reflection sessions, with tool design adapted to each mode.

The cross-material experiment reveals the essential role of knowledge quality, and that recipe replication — copying parameters from the highest-performing prior result rather than reasoning about their applicability — is an anti-pattern triggered by recipe availability. In all six same-material iron sessions, the agent selected the deprecated `dis_froz_max` value by extracting it from the best-performing result record, ignoring deprecation warnings. On unfamiliar nickel, the absence of a material-specific recipe forced the agent to reason from principles — and it achieved comparable or better accuracy. Knowledge systems should encourage principle-level entries over numerical recipes.

The QMatSuite architecture demonstrates robust generality across engines (QE, Wannier90 and ORCA) and models (Claude and GPT). Its engine-agnostic core provides the structural foundation for cross-engine knowledge transfer, establishing a clear trajectory for future multi-code autonomy. While our current analysis establishes learning causality through traceable, mechanistic behavioral changes, large-scale statistical profiling represents a promising next step as inference costs decline. To overcome the context-window limits of current models, QMatSuite leverages its graded knowledge hierarchy as a natural compression mechanism. This design ensures the system is natively scalable, transitioning seamlessly from managing dozens of individual findings to thousands of consolidated entries—an evolution that defines a robust new direction for high-capacity scientific memory systems, calling for future large-scale studies to further stress-test and refine its hierarchical boundaries.

A natural question is whether sufficiently capable models would obviate the need for knowledge infrastructure. Our experiments suggest the opposite: Claude Opus 4.6 already demonstrates sophisticated physical reasoning — discovering adaptive mesh refinement, performing systematic convergence studies, overriding incorrect inherited knowledge from computational evidence. The bottleneck is not reasoning capability but session isolation. Smarter models will record higher-quality insights, perform sharper reviews, and extract more transferable principles — making knowledge infrastructure more valuable, not less.

QMatSuite is fully open-source, requires no cloud services, and connects any AI model via the Model Context Protocol. The knowledge architecture supports community-contributed, domain-specific knowledge packs: a research group that spends months characterizing perovskite calculations can publish their accumulated knowledge as structured, provenance-backed data — the compressed, reviewed, and curated distillation of their experience — enabling any other group’s agent to start from that collective expertise rather than from zero [18]. Persistent scientific memory, demonstrated here for computational materials science, represents a general requirement for AI-driven research in any computational domain.

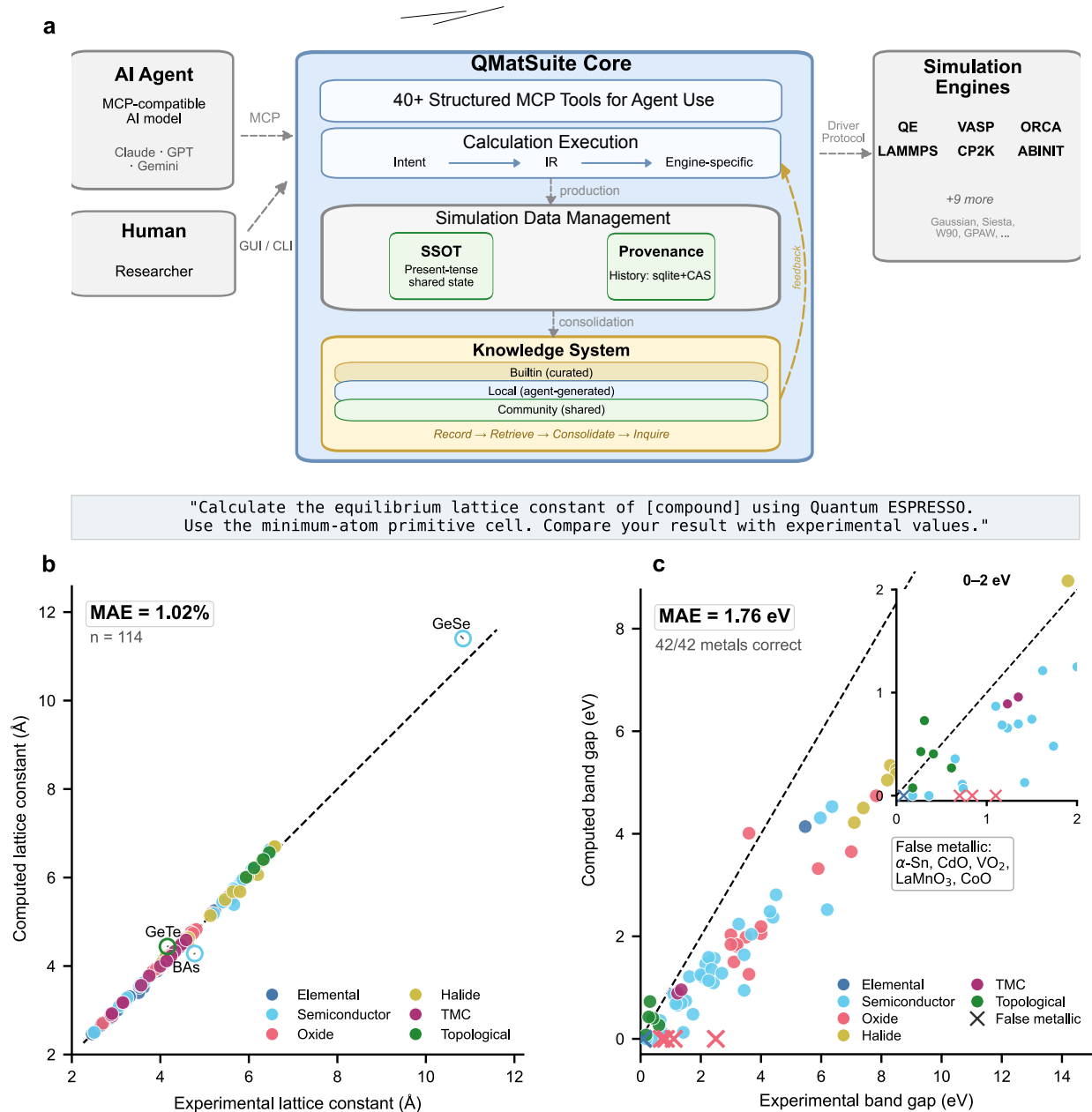


Figure 1: **Platform architecture and scale validation.** **a**, QMatSuite architecture showing symmetric access by AI agents (via MCP) and human researchers (via GUI) to the shared core, which contains the knowledge system, provenance tracking, present-tense shared state, and engine dispatch layer. **b**, Computed versus experimental lattice constants for 114 materials (MAE = 1.02%). **c**, Computed versus experimental band gaps for 68 non-metallic compounds (MAE = 1.76 eV); 42/42 metals correctly identified; 5 correlated insulators predicted metallic (known PBE limitation, marked \times). Inset: 0–2 eV region.

"Compute the Anomalous Hall Conductivity (AHC) of bcc Iron (Fe) using Quantum ESPRESSO and Wannier90. Use the primitive cell (1 atom). Compare your result with standard literature values and iterate until you get a reasonable result."

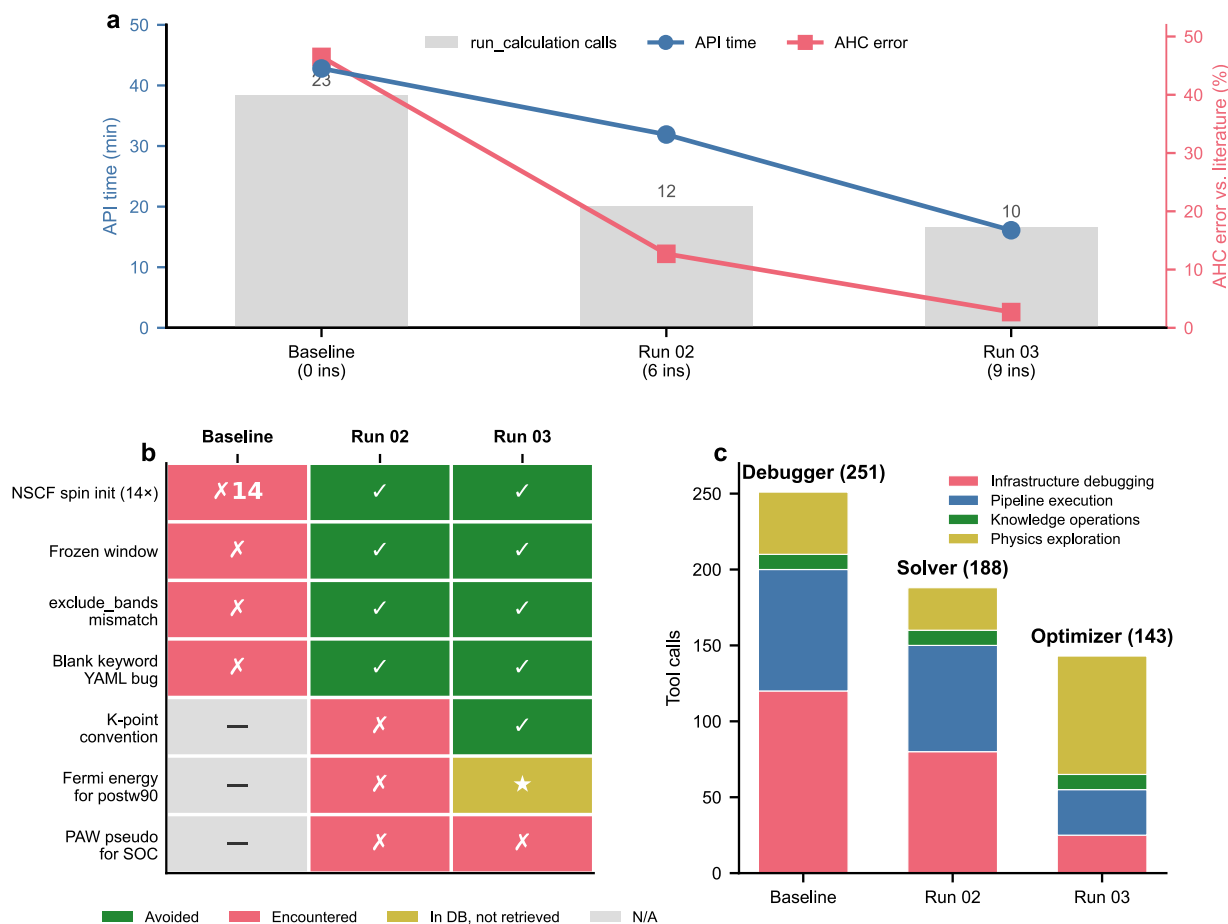
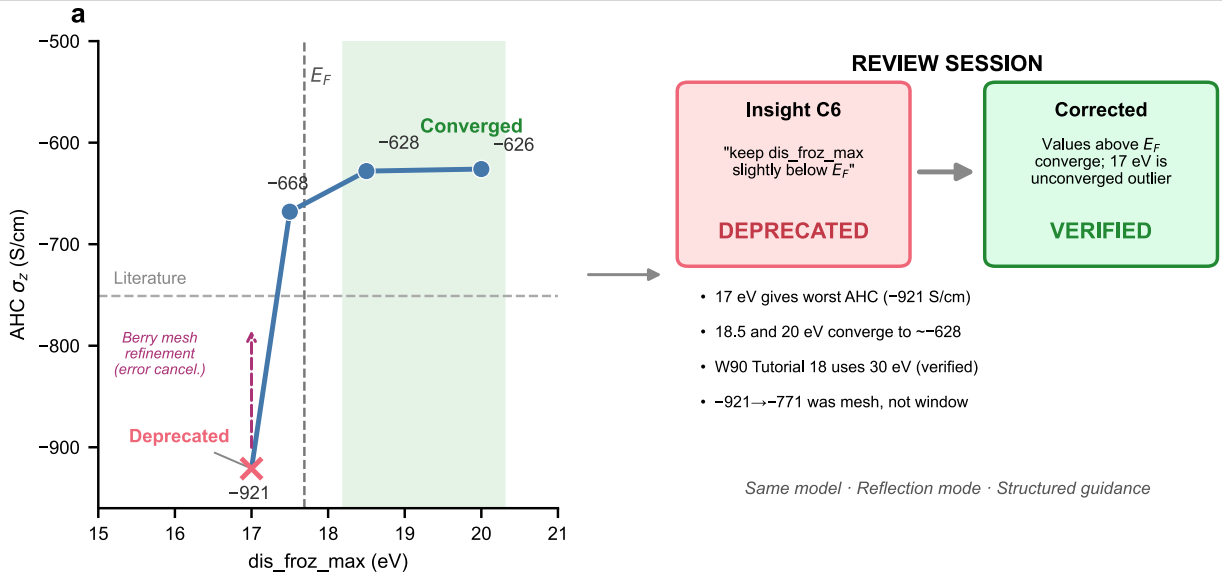
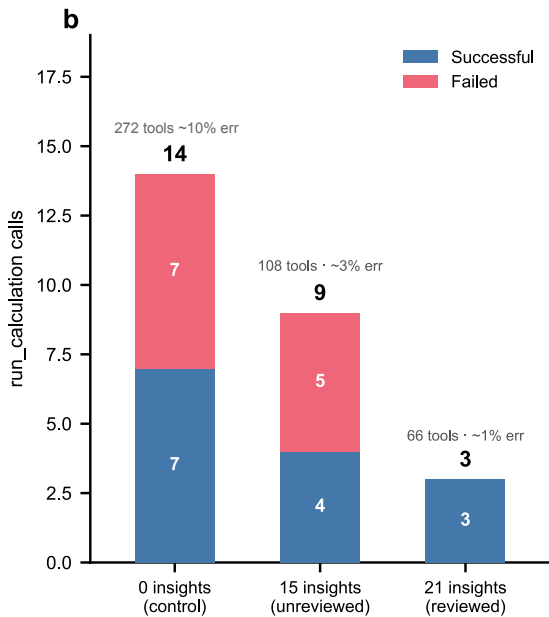


Figure 2: **Knowledge transforms a complex workflow.** **a**, Fe AHC learning curve across three runs with 0, 6, and 9 accumulated insights. Gray bars: `run_calculation` calls; blue line: API reasoning time; red line: AHC error versus literature. **b**, Episode avoidance matrix showing which pitfalls each run encountered (red) versus avoided via knowledge (green). Yellow: insight in database but not retrieved; gray: not applicable. **c**, Tool call composition shifting from infrastructure debugging (“Debugger”) to physics exploration (“Optimizer”).

"Review all findings in the knowledge base. Confirm, revise, or deprecate each based on your assessment."



"Compute the Anomalous Hall Conductivity (AHC) of fcc Nickel (Ni) using Quantum ESPRESSO and Wannier90. Use the primitive cell (1 atom). Compare your result with standard literature values and iterate until you get a reasonable result."



Same material · Same prompt · Same model · Knowledge varies

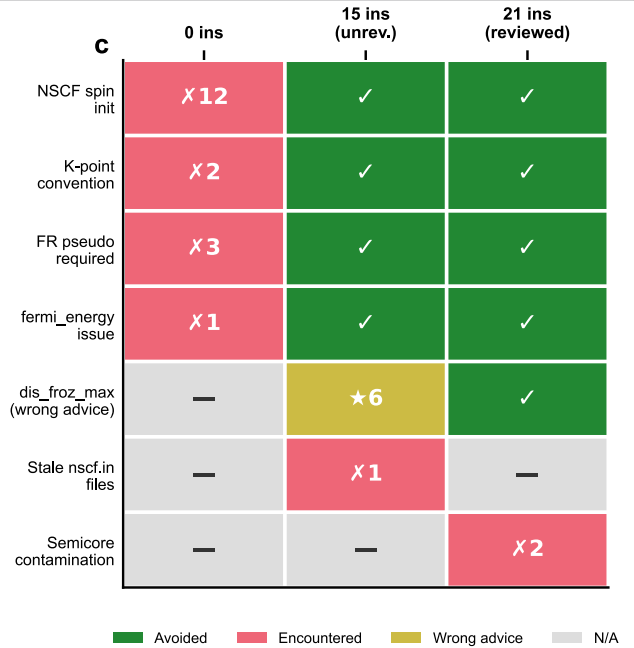


Figure 3: **Knowledge self-corrects and transfers across materials.** **a**, Left: convergence analysis showing the deprecated parameter recommendation ($\text{dis_froz_max} = 17$ eV, red \times) as an unconverged outlier, with the upward arrow indicating that Berry mesh refinement coincidentally pulled the AHC toward the literature value (error cancellation). Right: the review session's deprecation reasoning and corrected replacement. **b**, Ni AHC three-way comparison: 0 insights (14 calculations, 7 failures), 15 unreviewed insights (9 calculations, 5 failures), 21 reviewed insights (3 calculations, 0 failures). **c**, Ni pitfall avoidance matrix showing progressive transfer; yellow star ($\star 6$) marks the dis_froz_max row where unreviewed knowledge provided incorrect advice requiring 3 extra iterations.

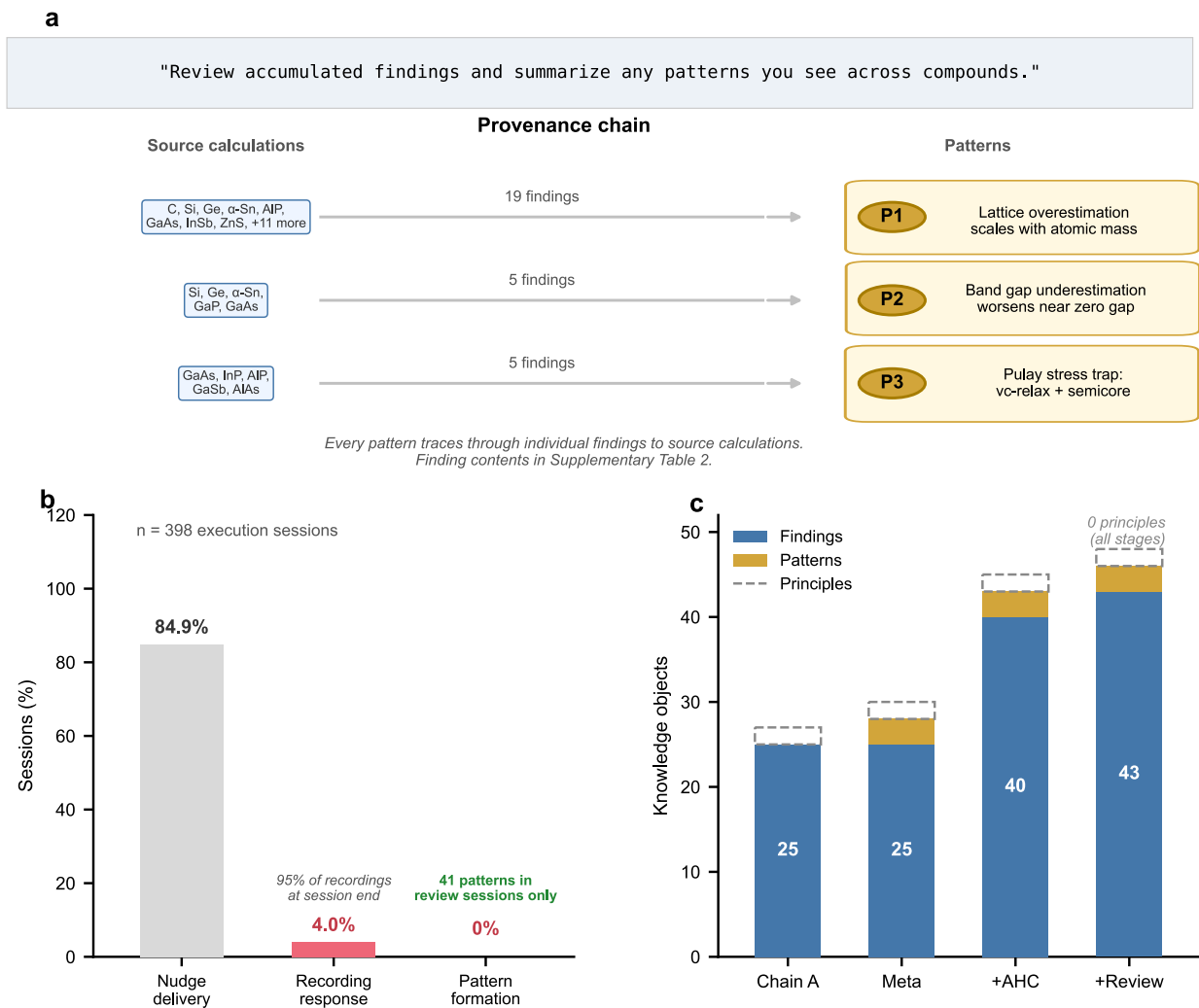


Figure 4: **Knowledge consolidates through dedicated reflection.** **a**, Three patterns distilled from 25 findings by a dedicated reflection session (Pattern 1: lattice overestimation scaling; Pattern 2: band gap underestimation; Pattern 3: Pulay stress trap), with provenance chains linking each pattern to its source calculations. **b**, Nudge compliance across 398 execution sessions: 84.9% received recording nudges, 4.0% showed any mid-session recording, 0% produced patterns during execution. All 41 patterns were produced exclusively in dedicated review sessions. **c**, Knowledge grade evolution across experiments: findings accumulate during execution (25→43), patterns appear only after dedicated reflection (0→3), principles remain an open frontier.

Methods

Platform architecture

QMatSuite provides 40+ structured tools via the Model Context Protocol (MCP), organized into five categories: Project (initialization, structure management), Config (parameter setting, presets), Execute (calculation launch, monitoring), Analysis (results extraction, structure promotion), and Knowledge (search, record, review). Engine drivers translate structured tool calls into engine-specific input files. Fifteen simulation engines are supported at varying integration levels: Quantum ESPRESSO [40, 41], VASP, ORCA, LAMMPS, CP2K, ABINIT, Gaussian, Siesta, Wannier90, GPAW, Psi4, PySCF, xTB, QMCPACK, and Yambo. All experiments in this work used Quantum ESPRESSO 7.5 [40, 41] with SSSP precision pseudopotentials [42] for solid-state calculations and ORCA 6.1.1 [24] for molecular calculations.

Persistent scientific memory

The knowledge system comprises three tiers stored in SQLite databases with FTS5 full-text search indexing. The builtin tier contains curated best practices (read-only). The local tier stores agent-generated insights (read-write) in three grades: findings (individual observations), patterns (cross-system regularities), and principles (general rules). Each entry includes scope tags, source calculation references, and free-text reasoning. The community tier supports sharable domain-specific insight packs. All tiers are searched via a unified `search_knowledge` tool with relevance ranking. Recording uses `record_insight` with mandatory grade, scope, and reasoning fields. Review uses `review_insight` with verdicts (confirmed, deprecated, promoted) and provenance links. Insights may reference other insights by ULID, enabling hierarchical knowledge structures.

AHC learning curve experiment (Exp 2)

The anomalous Hall conductivity of bcc iron was computed using the Quantum ESPRESSO + Wannier90 six-step pipeline: SCF \rightarrow NSCF \rightarrow wannierprep \rightarrow pw2wannier90 \rightarrow wannier90 \rightarrow postw90. The agent was Claude Opus 4.6 with no timeout. The prompt was identical across all three runs. Each run used a fresh Claude session, a fresh project directory, and the same model. The sole variable was the knowledge database: Condition A started empty (0 insights), Run 02 inherited 6 insights, and Run 03 inherited 9. The builtin knowledge database was disabled (`QMS_KNOWLEDGE_BUILTIN=0`) to isolate local knowledge effects. To ensure the knowledge database is the sole information channel between sessions, web search tools were blocked, engine installation tutorial and example files were removed from disk, and session persistence was disabled. All agent traces were audited post-hoc to verify that no external information sources — web, filesystem tutorials, or cached content from prior runs — were accessed in any experimental session. The model’s pre-training knowledge constitutes an uncontrolled stochastic baseline; the learning curve design (identical model, identical prompt, only the database content varying) isolates the database contribution from this baseline. All tool call counts were derived by parsing `trace.jsonl` as structured JSON, counting only `type=="tool_use"` content blocks within assistant messages.

Cross-material transfer experiment (Exp 2, Ni)

Three Ni AHC runs used the same prompt (substituting “fcc Nickel (Ni)” for the Fe element) and the same model (Claude Opus 4.6, no timeout). The baseline (0 insights) used an empty knowledge database with all leakage channels blocked; the trace was audited post-hoc to confirm no

external information access. Run 26 (15 insights) used the unreviewed Fe knowledge database containing two incorrect parameter recommendations. Run 24 (21 insights) used the reviewed database with deprecated entries corrected. The literature reference for fcc Ni AHC is approximately 2000–2400 S/cm [29, 31, 43, 44].

Meta session and knowledge consolidation experiment (Exp 3)

19 zinc-blende semiconductors underwent sequential relaxation and band structure calculations (24 sessions, Claude Opus 4.6) accumulating 25 findings in the local knowledge database. Two independent reflection sessions — one using Claude Sonnet 4.6, one using Claude Opus 4.6 — were then run with an identical 12-word prompt. Both models produced 3 patterns with identical themes, confirming that pattern structure is latent in the data rather than model-specific. A subsequent design experiment session (Claude Opus 4.6) used a 29-word prompt with no preamble, attempt limits, or tool instructions.

Nudge compliance analysis

Nudge compliance was measured across 398 execution sessions (270 from Exp 1, 128 from Exps 2–3) by parsing all `trace.jsonl` files programmatically. Recording nudge delivery was identified by matching nudge phrases in tool response text. Each `record_insight` call was located by event index within its session and classified by position (early <30%, mid 30–70%, late 70–90%, end-of-session >90%). Of 398 sessions, 338 (84.9%) received at least one recording nudge; 16 (4.0%) contained any mid-session `record_insight` call; 95.3% of all recordings occurred in the final 10% of session events; and zero sessions produced pattern-grade entries. All 41 patterns in the knowledge base were produced exclusively in dedicated review sessions.

Cross-engine molecular validation (ORCA + GPT 5.4)

98 molecules spanning diatomics, triatomics, small polyatomics, organics, radicals, and transition metal complexes were computed using ORCA 6.1.1 with agent-selected methods (predominantly B3LYP/def2-TZVP-level hybrid DFT [26, 45]). The agent was GPT 5.4 (OpenAI). Experimental reference bond lengths and angles were compiled from NIST CCCBDB, the NIST Chemistry WebBook, Huber & Herzberg spectroscopic constants, and primary spectroscopic literature.

Data availability

All experimental data including trace files, knowledge database snapshots, and computed results will be deposited at a public repository upon publication.

Code availability

QMatSuite is open-source and available at <https://github.com/QMatSuite> (GitHub) and <https://pypi.org/project/qmatsuite/> (PyPI).

Extended Data

Table 1: **Extended Data Table 1 | Comparison of AI agent systems for computational science.** Eight systems evaluated across capability dimensions relevant to knowledge-driven research. “Intent-level tools” means the agent expresses scientific purpose (e.g. `run_calculation`) rather than writing engine-specific input files. Knowledge persistence refers to whether agent-generated findings survive across independent sessions.

System	Venue	Input gen.	Param select.	Error recovery	Cross-session knowledge	Knowledge review	Engines	Open src
El Agente Q	<i>Matter</i> 2025	ORCA files	✓	✓	Static rules*	—	1	No
ChemGraph	<i>Commun. Chem.</i> 2026	ASE API	Partial	Limited	None	—	6	Yes
DREAMS	arXiv 2025	QE via ASE	✓	✓	Session-scoped	—	1	Yes
AtomAgents	<i>PNAS</i> 2025	Pre-built fn	Partial	Limited	None	—	1	Yes
VASPIlot	<i>Chin. Phys. B</i> 2025	VASP files	Hybrid	✓	RAG (wiki)	—	1	Yes
Masgent	arXiv 2025	VASP files	Defaults	Preventive	None	—	1	Yes
Aitomia	arXiv 2025	✓	✓	✓	None	—	ML	Partial
QMatSuite	This work	Intent tools	✓	✓	Persistent, graded	✓	15	Yes

*El Agente Q’s “hierarchical memory” consists of static rules manually curated by human experts; episodic memory is explicitly disabled in the published implementation.

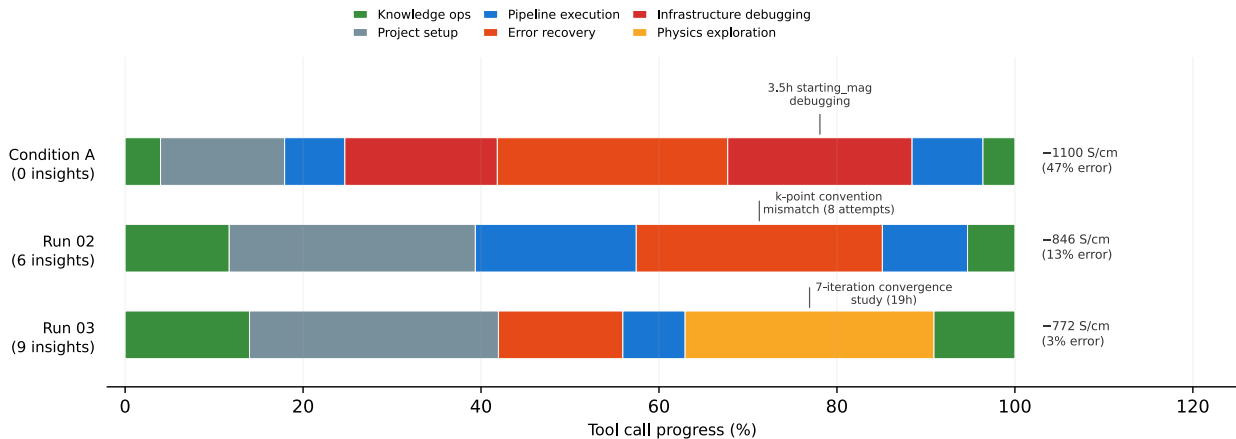


Figure 5: **Extended Data Fig. 1 | Temporal structure of agent activity across three Fe AHC runs.** Gantt-style visualization of tool call composition, showing the shift from infrastructure debugging to physics exploration as knowledge accumulates. **Condition A** (0 insights): dominated by debugging and error recovery, with 3.5 hours spent diagnosing why the computed AHC was zero (the `starting_magnetization` issue). The agent timed out at 6.2 hours. **Run 02** (6 insights): proactively avoided the `starting_mag` pitfall but encountered a novel `k-point convention mismatch` requiring 8 attempts. **Run 03** (9 insights): resolved all setup issues within the first 80 tool calls, then devoted the remainder to a voluntary 7-iteration convergence study exploring disentanglement parameters and adaptive mesh refinement — a qualitative shift from “getting it to work” to “understanding the physics.” Results shown at right demonstrate monotonic accuracy improvement.

Table 2: **Extended Data Table 2 | All 15 insights accumulated across the iron AHC learning curve.** Each entry shows the verbatim content (truncated), source run, type, and correctness assessment. Of 15 insights, 13 are fully correct, 1 partially correct (A5: correct calculation, incomplete convergence attribution), and 1 contains correct data but an incorrect conclusion (C6: dis_froz_max recommendation based on unconverged outlier). C6 was deprecated in a dedicated review session and replaced with a corrected version.

ID	Run	Content (excerpt)	Type	Correct?	Review
A1	Baseline	Frozen window error: dis_froz_max must be below energy where band count > num_wann	Error fix	✓	Verified
A2	Baseline	CRITICAL: NSCF must include starting_magnetization with SOC or Berry curvature = 0	Error fix	✓	Verified
A3	Baseline	Semicore exclusion: set dis_froz_min=5 eV to exclude 3s3p bands	Error fix	✓	Verified
A4	Baseline	exclude_bands causes .eig mismatch with pw2wannier90	Error fix	✓	Confirmed
A5	Baseline	AHC result: $\sigma_z = -1100$ S/cm, $8 \times 8 \times 8$ grid, 47% error	Result	Partial	Confirmed
A6	Baseline	Setting exclude_bands='' crashes Wannier90	Error fix	✓	Confirmed
B1	Run 02	K-point convention: QE uses [0, 1), Wannier90 uses [-0.5, 0.5); provide explicit list	Error fix	✓	Verified
B2	Run 02	postw90 berry=true requires fermi_energy parameter	Error fix	✓	Confirmed
B3	Run 02	AHC result: $\sigma_z = -846$ S/cm, $10 \times 10 \times 10$ grid, 13% error	Result	✓	Confirmed
C1	Run 03	Projections must be plain string, not nested list	Error fix	✓	Confirmed
C2	Run 03	fermi_energy required (redundant with B2)	Error fix	✓	Confirmed
C3	Run 03	SOC requires FR pseudopotentials (not PAW)	Error fix	✓	Verified
C4	Run 03	Best AHC: $\sigma_z = -772$ S/cm, adaptive mesh, 3% error	Result	✓	Confirmed
C5	Run 03	Adaptive refinement \gg brute-force mesh (1/7 cost, better accuracy)	Method	✓	Confirmed
C6	Run 03	dis_froz_max sensitivity: keep below E_F	Method	Wrong[†]	Deprecated

[†]C6 contains correct sensitivity data but draws an incorrect conclusion: dis_froz_max=17 produced the best AHC (-921 S/cm) through error cancellation (Berry mesh refinement compensated for unconverged Wannier functions). Higher values (18.5, 20) converge to ~ -628 S/cm. Deprecated and replaced in review session.

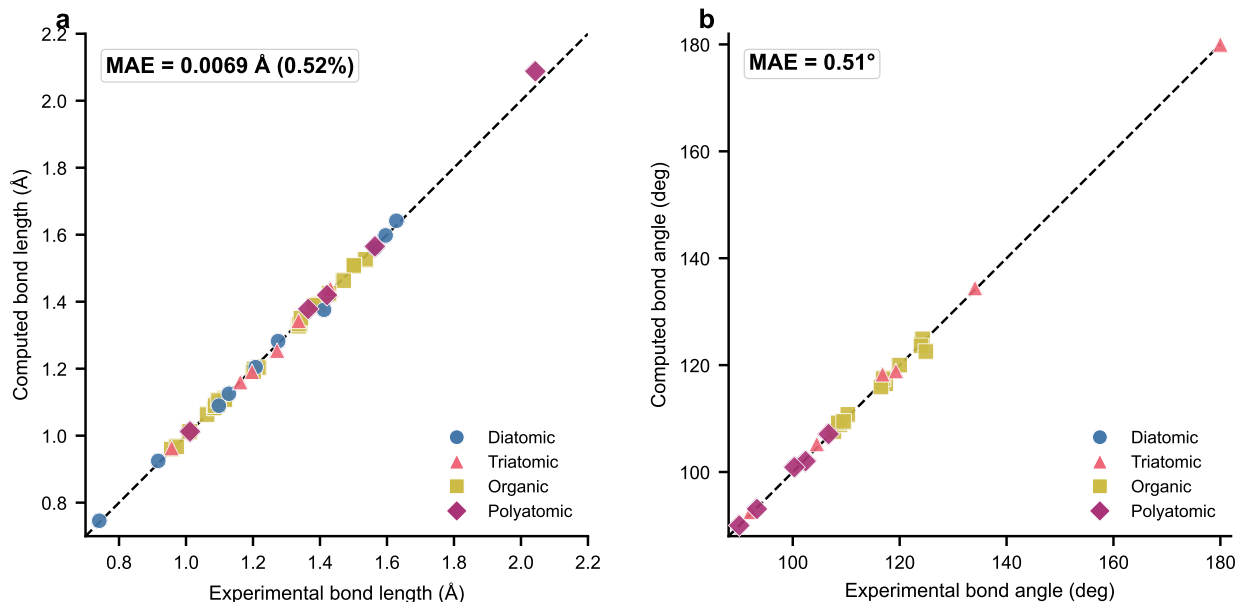


Figure 6: **Extended Data Fig. 2 | Cross-engine, cross-model validation: molecular geometry optimization with ORCA 6.1.1 and GPT 5.4.** **a**, Computed versus experimental bond lengths for 78 comparisons from the reference-backed raw-ORCA-converged subset (MAE = 0.0069 Å, 0.52%), consistent with established hybrid-DFT benchmarks. **b**, Computed versus experimental bond angles for 33 comparisons (MAE = 0.51°). This experiment uses a different simulation engine (ORCA vs Quantum ESPRESSO), a different AI model (GPT 5.4 vs Claude), and a different chemical domain (molecular vs solid-state), confirming that the platform generalizes across all three axes. Of 98 molecules, 91 completed under the conservative publication criterion; the seven final failures comprise two agent-declared failures despite converged raw outputs, three missing or non-terminated last-output cases, and two explicit last-attempt error terminations.

Table 3: **Extended Data Table 3 | Insight retrieval and application across AHC runs.** Matrix showing which insights from the knowledge database were retrieved and applied in each run. Green cells indicate successful knowledge transfer; yellow (★) marks an insight present in the database but not retrieved, causing the agent to re-encounter the corresponding error. This case (insight B2 in Run 03) provides causal evidence that retrieval — not latent model knowledge — mediates transfer: the same model with the same pre-training failed to avoid an error whose solution was available but not found by BM25 search.

ID	Content (brief)	Run 02		Run 03	
		Retrieved	Applied	Retrieved	Applied
A1	Frozen window fix	✓	✓	—	—
A2	starting_mag (CRITICAL)	✓	✓	✓	✓
A3	Semicore exclusion	—	Set indep.	✓	✓
A4	exclude_bands trap	✓	Avoided	—	—
A5	AHC −1100 (prior result)	✓	Planning	✓	Planning
A6	Blank keyword bug	✓	Avoided	—	—
B1	K-point convention	<i>(Recorded this run)</i>		✓	✓
B2	fermi_energy required	<i>(Recorded this run)</i>		★ Not retr.	Hit error
B3	AHC −846 (improved)	<i>(Recorded this run)</i>		✓	Planning

★ Insight B2 was in the database but none of Run 03’s four search queries matched it. The agent independently resolved the error and recorded a redundant insight (C2). This demonstrates that BM25 retrieval is imperfect — having knowledge in the database does not guarantee it will be found.

References

- [1] Daniil A. Boiko, Robert MacKnight, Ben Kline, and Gabe Gomes. Autonomous chemical research with large language models. *Nature*, 624(7992):570–578, 2023.
- [2] Andres M. Bran, Sam Cox, Oliver Schilter, Carlo Baldassari, Andrew D. White, and Philippe Schwaller. Augmenting large language models with chemistry tools. *Nat. Mach. Intell.*, 6(5):525–535, 2024.
- [3] Alireza Ghafarollahi and Markus J. Buehler. Automating alloy design and discovery with physics-aware multimodal multiagent AI. *Proc. Natl Acad. Sci. USA*, 122(4):e2414074122, 2025.
- [4] Yunheng Zou, Austin H. Cheng, Abdulrahman Aldossary, Jiaru Bai, Shi Xuan Leong, Jorge Arturo Campos-Gonzalez-Angulo, Changhyeok Choi, Cher Tian Ser, Gary Tom, Andrew Wang, Zijian Zhang, Ilya Yakavets, Han Hao, Chris Crebolder, Varinia Bernales, and Alán Aspuru-Guzik. El Agente: An autonomous agent for quantum chemistry. *Matter*, 8(7):102263, 2025.
- [5] Ignacio Gustin, Luis Mantilla Calderón, Juan B Pérez-Sánchez, Jérôme F Gonthier, Yuma Nakamura, Karthik Panicker, Manav Ramprasad, Zijian Zhang, Yunheng Zou, Varinia Bernales, et al. El agente cu\`antico: Automating quantum simulations. *arXiv preprint arXiv:2512.18847*, 2025.
- [6] Juan B Pérez-Sánchez, Yunheng Zou, Jorge A Campos-Gonzalez-Angulo, Marcel Müller, Ignacio Gustin, Andrew Wang, Han Hao, Tsz Wai Ko, Changhyeok Choi, Eric S Isbrandt, et al. El agente quntur: A research collaborator agent for quantum chemistry. *arXiv preprint arXiv:2602.04850*, 2026.
- [7] Sai Govind Hari Kumar, Yunheng Zou, Andrew Wang, Jesús Valdés-Hernández, Tsz Wai Ko, Nathan Yue, Olivia Leng, Hanyong Xu, Chris Crebolder, Alán Aspuru-Guzik, et al. El agente s\`olido: A new age (nt) for solid state simulations. *arXiv preprint arXiv:2602.17886*, 2026.
- [8] Jiaru Bai, Abdulrahman Aldossary, Thomas Swanick, Marcel Müller, Yeonghun Kang, Zijian Zhang, Jin Won Lee, Tsz Wai Ko, Mohammad Ghazi Vakili, Varinia Bernales, et al. El agente gr\`afico: Structured execution graphs for scientific agents. *arXiv preprint arXiv:2602.17902*, 2026.
- [9] Thang D. Pham, Aditya Tanikanti, and Murat Keçeli. ChemGraph as an agentic framework for computational chemistry workflows. *Commun. Chem.*, 9:33, 2026.
- [10] Ziqi Wang, Hongshuo Huang, Hancheng Zhao, Changwen Xu, Shang Zhu, Jan Janssen, and Venkatasubramanian Viswanathan. DREAMS: Density functional theory based research engine for agentic materials simulation. 2025.
- [11] Jiaxuan Liu, Tiannian Zhu, Caiyuan Ye, Zhong Fang, Hongming Weng, and Quansheng Wu. VASPilot: MCP-facilitated multi-agent intelligence for autonomous VASP simulations. *Chinese Phys. B*, 34(11):117106, 2025.
- [12] Guangchen Liu, Songge Yang, and Yu Zhong. Masgent: An AI-assisted materials simulation agent. 2025.
- [13] Patrick Lewis et al. Retrieval-augmented generation for knowledge-intensive NLP tasks. 2020.

- [14] Yuyang Hu, Shichun Liu, Yanwei Yue, Guibin Zhang, Boyang Liu, Fangyi Zhu, Jiahang Lin, Honglin Guo, Shihan Dou, Zhiheng Xi, Senjie Jin, Jiejun Tan, Yanbin Yin, Jiongnan Liu, Zeyu Zhang, Zhongxiang Sun, Yutao Zhu, Hao Sun, Boci Peng, Zhenrong Cheng, Xuanbo Fan, Jiabin Guo, Xinlei Yu, Zhenhong Zhou, Zewen Hu, Jiahao Huo, Junhao Wang, Yuwei Niu, Yu Wang, Zhenfei Yin, Xiaobin Hu, Yue Liao, Qiankun Li, Kun Wang, Wangchunshu Zhou, Yixin Liu, Dawei Cheng, Qi Zhang, Tao Gui, Shirui Pan, Yan Zhang, Philip Torr, Zhicheng Dou, Ji-Rong Wen, Xuanjing Huang, Yu-Gang Jiang, and Shuicheng Yan. Memory in the age of AI agents. 2025.
- [15] Anthropic. Model context protocol, 2024. Open standard for AI model–tool integration.
- [16] Sebastiaan P. Huber, Spyros Zoupanos, Martin Uhrin, Leopold Talirz, Leonid Kahle, Rico Häuselmann, Dominik Gresch, Tiziano Müller, Aliaksandr V. Yakutovich, Casper W. Andersen, Francisco F. Ramirez, Carl S. Adorf, Fernando Gargiulo, Snehal Kumbhar, Elsa Passaro, Conrad Johnston, Andrius Merkys, Andrea Cepellotti, Nicolas Mounet, Nicola Marzari, Boris Kozinsky, and Giovanni Pizzi. AiiDA 1.0, a scalable computational infrastructure for automated reproducible workflows and data provenance. *Sci. Data*, 7:300, 2020.
- [17] Anubhav Jain et al. FireWorks: a dynamic workflow system designed for high-throughput applications. *Concurrency Computat.: Pract. Exper.*, 27(17):5037–5059, 2015.
- [18] Mark D. Wilkinson et al. The FAIR guiding principles for scientific data management and stewardship. *Sci. Data*, 3:160018, 2016.
- [19] John P. Perdew, Kieron Burke, and Matthias Ernzerhof. Generalized gradient approximation made simple. *Phys. Rev. Lett.*, 77:3865–3868, 1996.
- [20] Kurt Lejaeghere et al. Reproducibility in density functional theory calculations of solids. *Science*, 351(6280):aad3000, 2016.
- [21] Philipp Haas, Fabien Tran, and Peter Blaha. Calculation of the lattice constant of solids with semilocal functionals. *Phys. Rev. B*, 79:085104, Feb 2009.
- [22] Paula Mori-Sánchez, Aron J. Cohen, and Weitao Yang. Localization and delocalization errors in density functional theory and implications for band-gap prediction. *Phys. Rev. Lett.*, 100:146401, 2008.
- [23] Aron J. Cohen, Paula Mori-Sánchez, and Weitao Yang. Insights into current limitations of density functional theory. *Science*, 321(5890):792–794, 2008.
- [24] Frank Neese et al. The ORCA quantum chemistry program package. *WIREs Comput. Mol. Sci.*, 10(6):e1459, 2020.
- [25] Michael Bühl and Hannes Kabrede. Geometries of transition-metal complexes from density-functional theory. *J. Chem. Theory Comput.*, 2(5):1282–1290, 2006.
- [26] Narbe Mardirossian and Martin Head-Gordon. Thirty years of density functional theory in computational chemistry: an overview and extensive assessment of 200 density functionals. *Mol. Phys.*, 115(19):2315–2372, 2017.
- [27] Naoto Nagaosa, Jairo Sinova, Shigeki Onoda, A. H. MacDonald, and N. P. Ong. Anomalous hall effect. *Rev. Mod. Phys.*, 82:1539–1592, May 2010.

- [28] Giovanni Pizzi, Valerio Vitale, Ryotaro Arita, Stefan Blügel, Frank Freimuth, Guillaume Géranton, Marco Gibertini, Dominik Gresch, Charles Johnson, Takashi Koretsune, Julen Ibañez-Azpiroz, Hyungjun Lee, Jae-Mo Lihm, Daniel Marchand, Antimo Marrazzo, Yuriy Mokrousov, Jamal I. Mustafa, Yoshiro Nohara, Yusuke Nomura, Lorenzo Paulatto, Samuel Poncé, Thomas Ponweiser, Junfeng Qiao, Florian Thöle, Stepan S. Tsirkin, Małgorzata Wierzbowska, Nicola Marzari, David Vanderbilt, Ivo Souza, Arash A. Mostofi, and Jonathan R. Yates. Wannier90 as a community code: new features and applications. *J. Phys.: Condens. Matter*, 32:165902, 2020.
- [29] Yugui Yao, Leonard Kleinman, A. H. MacDonald, Jairo Sinova, T. Jungwirth, Ding-sheng Wang, Enge Wang, and Qian Niu. First principles calculation of anomalous Hall conductivity in ferromagnetic bcc Fe. *Phys. Rev. Lett.*, 92:037204, 2004.
- [30] Ivo Souza, Nicola Marzari, and David Vanderbilt. Maximally localized wannier functions for entangled energy bands. *Phys. Rev. B*, 65:035109, Dec 2001.
- [31] Xinjie Wang, David Vanderbilt, Jonathan R Yates, and Ivo Souza. Fermi-surface calculation of the anomalous hall conductivity. *Physical Review B—Condensed Matter and Materials Physics*, 76(19):195109, 2007.
- [32] GP Francis and Mike C Payne. Finite basis set corrections to total energy pseudopotential calculations. *Journal of Physics: Condensed Matter*, 2(19):4395–4404, 1990.
- [33] Ut Na Sio and Thomas C. Ormerod. Does incubation enhance problem solving? a meta-analytic review. *Psychol. Bull.*, 135(1):94–120, 2009.
- [34] Benjamin Baird, Jonathan Smallwood, Michael D. Mrazek, Jason W. Y. Kam, Michael S. Franklin, and Jonathan W. Schooler. Inspired by distraction: mind wandering facilitates creative incubation. *Psychol. Sci.*, 23(10):1117–1122, 2012.
- [35] Taiwei Shi, Sihao Chen, Bowen Jiang, Linxin Song, Longqi Yang, and Jieyu Zhao. Experiential reinforcement learning. 2026.
- [36] Nelson F. Liu et al. Lost in the middle: How language models use long contexts. *Trans. Assoc. Comput. Linguist.*, 12:157–173, 2024.
- [37] Charles Packer et al. MemGPT: Towards LLMs as operating systems. 2023.
- [38] Joon Sung Park, Joseph C. O’Brien, Carrie J. Cai, Meredith Ringel Morris, Percy Liang, and Michael S. Bernstein. Generative agents: Interactive simulacra of human behavior. In *Proceedings of the 36th Annual ACM Symposium on User Interface Software and Technology*, 2023.
- [39] Noah Shinn, Federico Cassano, Ashwin Berman, Kush Gopinath, Karthik Narasimhan, and Shunyu Yao. Reflexion: Language agents with verbal reinforcement learning. 2023.
- [40] Paolo Giannozzi, Stefano Baroni, Nicola Bonini, Matteo Calandra, Roberto Car, Carlo Cavazzoni, Davide Ceresoli, Guido L. Chiarotti, Matteo Cococcioni, Ismaila Dabo, Andrea Dal Corso, Stefano de Gironcoli, Stefano Fabris, Guido Fratesi, Ralph Gebauer, Uwe Gerstmann, Christos Gougoussis, Anton Kokalj, Michele Lazzeri, Layla Martin-Samos, Nicola Marzari, Francesco Mauri, Riccardo Mazzarello, Stefano Paolini, Alfredo Pasquarello, Lorenzo Paulatto, Carlo Sbraccia, Sandro Scandolo, Gabriele Sclauzero, Ari P. Seitsonen, Alexander Smogunov, Paolo

- Umari, and Renata M. Wentzcovitch. QUANTUM ESPRESSO: a modular and open-source software project for quantum simulations of materials. *J. Phys.: Condens. Matter*, 21:395502, 2009.
- [41] Paolo Giannozzi, Oliviero Andreussi, Thomas Brumme, Oana Bunau, Marco Buongiorno Nardelli, Matteo Calandra, Roberto Car, Carlo Cavazzoni, Davide Ceresoli, Matteo Cococcioni, Nicola Colonna, Ivan Carnimeo, Andrea Dal Corso, Stefano de Gironcoli, Pietro Delugas, Robert A. DiStasio, Andrea Ferretti, Andrea Floris, Guido Fratesi, Giorgia Fugallo, Ralph Gebauer, Uwe Gerstmann, Feliciano Giustino, Tommaso Gorni, Junteng Jia, Mitsuaki Kawamura, Hsin-Yu Ko, Anton Kokalj, Emine Küçükbenli, Michele Lazzeri, Matteo Marsili, Nicola Marzari, Francesco Mauri, Ngoc Linh Nguyen, Hai-Van Nguyen, Alberto Otero-de-la Roza, Lorenzo Paulatto, Samuel Poncé, Dario Rocca, Riccardo Sabatini, Biswajit Santra, Martin Schlipf, Ari P. Seitsonen, Alexander Smogunov, Iurii Timrov, Timo Thonhauser, Paolo Umari, Nathalie Vast, Xifan Wu, and Stefano Baroni. Advanced capabilities for materials modelling with Quantum ESPRESSO. *J. Phys.: Condens. Matter*, 29:465901, 2017.
- [42] Gianluca Prandini, Antimo Marrazzo, Ivano E. Castelli, Nicolas Mounet, and Nicola Marzari. Precision and efficiency in solid-state pseudopotential calculations. *npj Comput. Mater.*, 4:72, 2018.
- [43] Huei-Ru Fuh and Guang-Yu Guo. Intrinsic anomalous hall effect in nickel: A gga+ u study. *Physical Review B—Condensed Matter and Materials Physics*, 84(14):144427, 2011.
- [44] Jakub Železný, Yuta Yahagi, Carles Gomez-Olivella, Yang Zhang, and Yan Sun. High-throughput study of the anomalous hall effect. *npj Computational Materials*, 9(1):151, 2023.
- [45] Florian Weigend and Reinhart Ahlrichs. Balanced basis sets of split valence, triple zeta valence and quadruple zeta valence quality for H to Rn: Design and assessment of accuracy. *Phys. Chem. Chem. Phys.*, 7:3297–3305, 2005.